Journal of Materials Chemistry A

Accepted Manuscript

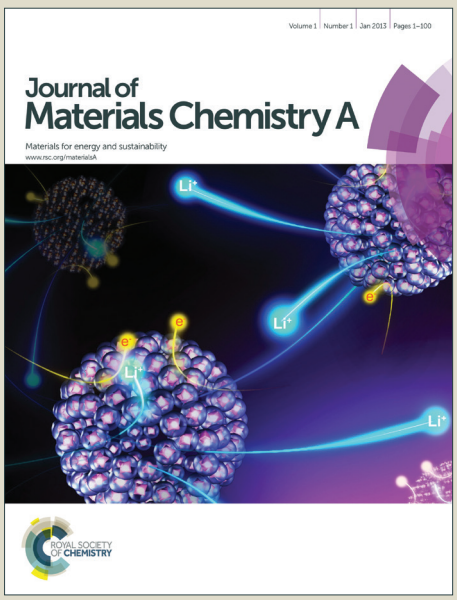

ROYAL SOCIETY OF CHEMISTRY

www.rsc.org/materialsA

Submerged liquid plasma – Low energy synthesis of nitrogen-doped graphene for electrochemical applications

Jaganathan Senthilnathan, Kodepelly Sanjeeva Rao, Masahiro Yoshimura*

Promotion Centre for Global Materials Research (PCGMR),

Department of Material Science and Engineering,

National Cheng Kung University, Tainan, Taiwan

Abstract

In this study, micro-plasma discharge is produced by applying a high electric potential between graphite and Pt electrodes in acetonitrile solvent. The electrons generated in the micro-plasma discharge collide with acetonitrile and produce ·H and $\cdot CH_2CN$ radicals. The radicalized graphene layer exfoliated from the graphite electrode reacts with nascent hydrogen (·H) and acetonitrile ($\cdot CH_2CN$) radicals and partially restores its aromaticity and conjugation. Raman spectra of the product confirm the synthesis of nitrogen-functionalized graphene (N-FG), which has a marginal increase in disorderness compared to that of pure graphite and remarkable dispersibility in both hydrophilic and hydrophobic solvents. The excellent fluorescence property of N-FG confirms the presence of fluorophores such as -NH and -N=C- at the radicalized graphene sites, as supported by ultraviolet-visible spectroscopy and X-ray photoelectron spectroscopy studies. The functional groups present in N-FG lead to excellent electrochemical performance, with distinct redox peaks in cyclic voltammetry and a high specific capacitance of 291 F/g at a scan rate of 5 mV/s. N-FG exhibits excellent cycling stability, with a marginal reduction of specific capacitance (<10% reduction) at the end of 1000 cycles.

Keywords: submerged liquid plasma, acetonitrile radical, functionalized graphene, supercapacitor, nascent hydrogen

1. Introduction

Graphene has been extensively studied due to its excellent properties for various industrial applications.[1-3] Large-scale synthesis of single-layer graphene is being constrained by its strong van der Waals force of attraction (π-π interactions) and leads to irreversible agglomeration in solution.[4-6] The functionalization of graphene is an important route for enhancing its stability and dispersibility in solvents.[7] Graphene oxide (GO) is an important functionalized product of graphene. However, high content of sp^3 carbon restricts electron mobility and leads to poor electrical properties.[8] The surface functionalization of graphene has been extensively carried out with organic moieties such as pyrrol, porphyrin, polyaniline, conjugative polymers, nafion, and o-phenylenediamine.[9-15] The chemically adsorbed or covalently bonded organic moieties are more susceptible to reacting with external impurities. Their long-term stability with graphene is thus highly questionable and requires further investigation.[16] Furthermore, organic polymer/graphene composites have low electrical conductivity and poor cycling stability, limiting their practical applications.[17] For functionalized graphene, the stability of covalent bonds with sp^2 carbon obtained with the insertion of heteroatoms such as nitrogen and boron is higher than that of surface adsorbed graphene/organic moiety composites.[16, 18] Nitrogen-doped graphene has been extensively studied due to its greater stability and dispersibility and enhanced electrochemical properties.[18] Nitrogen insertion in graphene forms pyridinic (sp^2-hybridized) or pyrrolic (sp^3-hybridized) bonding configurations by donating one or two p electrons to the π system.[18] The pyridinic and pyrrolic nitrogen present in graphene displays remarkable capacitance property called faradaic supercapacitors or pseudocapacitors.[19] The formation of functionalized graphene is complicated by the high temperature and toxic chemicals used in

chemical vapor deposition, gas plasma or glow discharge plasma deposition, segregation growth, thermal annealing, microwave plasma deposition, solvothermal synthesis, arc discharge method, and thermal exfoliation, all of which require harsh conditions (Fig. 1).[16, 20-29] The most important aspect of graphene functionalization is to retain its aromaticity and enhance its dispersibility in solvents. Furthermore, the large-scale synthesis of functionalized graphene should use a sustainable, economical, and eco-friendly process. The present study thus applies the submerged liquid plasma (SLP) process for the direct synthesis of functionalized graphene in acetonitrile solvent. The electrocapacitive properties of as-prepared nitrogen-functionalized graphene (N-FG) and its cyclic stability are evaluated using a three-electrode electrochemical cell.

2. Experimental section

2.1 Experimental setup

All experiments were conducted using Pt and graphite rod (99.99%) electrodes. The tip diameter of the graphite rod was maintained at 200-800 µm. Acetonitrile (99.95%) and the graphite rod (diameter: 6.15 mm; length: 152 mm) (AGKSP grade, ultra "F" purity) procured from Alfa Aesar were used as the target materials. A discharge voltage of 2.9 kV was applied with a repetition rate of 10 kHz, a pulse delay of 500 µs, and a pulse width of 5 ms across the electrodes using a pulse generator (AVTECH AV-1022-C) connected to a high-voltage amplifier (TREK Model 609E-6), which can generate 0.1 to 5 kV. To get the maximum plasma intensity, the distance between the graphite and Pt electrodes was maintained at ~75 µm by using a moving stage assembly (Translation Stage Triple-Divide Series 9064 and 9065) operated by a computer. A submerged plasma reaction in acetonitrile was carried out for a fixed

reaction time of 30 min. The final N-FG solution was centrifuged (8000 rpm) and the residue was washed with acetonitrile solution several times.

2.2 Characterizations

The absorption spectrum of N-FG was collected using an ultraviolet-visible (UV-Vis) spectrometer (SCINCO S-3100). Raman spectroscopy analysis was performed using a confocal micro-Raman spectrometer (Renishaw inVia) with a 633-nm argon laser as the excitation source. The microstructure and surface morphology of N-FG were monitored using a high-resolution transmission electron microscope (HR-TEM, JEOL JEM 2100F) operated at 200 kV. The fluorescence spectrum of N-FG was recorded with a fluorescence spectrophotometer (Hitachi F-4500). The Fourier transform-infrared (FT-IR) spectrum of N-FG was recorded using the KBr disk method (Nicolet Nexus 470) with 30 scans for each sample at a 4 cm^{-1} spectral resolution. High-resolution X-ray photoelectron spectroscopy (HRXPS, PHI Quantera SXM, ULVAC Inc) was used to analyze the binding energies of carbon and nitrogen present in N-FG.

2.3 Cyclic voltammetry

The electrocapacitive property of N-FG was evaluated with cyclic voltammetry (CV) in 6 M KOH at room temperature using a potentiostat (AUTOLAB PGSTAT 302). The experiments were carried out with a conventional three-electrode system. The working electrode was prepared using a 9:1 weight ratio of N-FG and polytetrafluoroethylene (PTFE) coated on fluorine-doped tin oxide (FTO) conducting glass. A Pt electrode was used as the counter electrode and a saturated calomel electrode (SCE) was used as the reference electrode. The potential was scanned in a

range of 0 to 0.4 V. The average specific capacitance was calculated as $Cs = \frac{qa+qb}{2m\Delta V}$, where *qa* and *qb* are the anodic and cathodic peak currents, respectively, *m* is the weight (~ 1 mg) of the active material coated on FTO (coated area ~ 1 cm^2), and ΔV is the change in voltage.

3. Results and discussion

3.1 Formation of N-FG in submerged liquid plasma process

When a high potential difference is applied across the graphite and platinum electrodes in acetonitrile solution, micro-plasma discharge occurs at the interface and leads to the flow of electrons between the electrodes (Fig. S1).[30-33] The micro-plasma discharge forms radicalized graphene sheets, which are exfoliated in the acetonitrile solvent instantly. The non-polar acetonitrile has no affinity towards radicalized carbon and prevents agglomeration, forming stable dispersion. The free electrons generated during micro-plasma discharge collide with acetonitrile and initiate hydrogen detachment, which results in highly reactive free radical monomers (·H and $\cdot CH_2$-C≡N).[34, 35] The nitrile group resists electron attack due to the high stability of -C≡N (891 kJ/mol) bond.[30] The C-H (413 kJ/mol) bond present in acetonitrile is more vulnerable to electron attack due to its lower bond energy compared to that of -C≡N.[30, 34, 35] Highly reactive nascent ·H effectively reacts with radicalized graphene and partially restores the sp^2 network. Similarly, the $\cdot CH_2$-C≡N radical reacts with the radicalized graphene layer and forms pyridinic and pyrrolic nitrogen. The pyridinic (-N=CH-) and pyrrolic (-NH) nitrogen act as intermittent terminal groups and cause marginal disorderness in the sp^2 carbon network. The pyridinic nitrogen is well inserted into the sp^2 network and partially restores the aromaticity and conjugation of the graphene

layers. The five-member pyrrolic nitrogen increases the sp^3 carbon content and brings disorderness into the graphene layer. The $\cdot CH_2\text{-}C\equiv N$ radical present in the solution may also initiate the formation of terminal-end aliphatic nitrogen or alkene ($CH_2\text{-}CH_2\text{-}CN$ or -CH=CH-CH=CH-) in the radicalized graphene layer. A schematic representation of micro-plasma discharge and graphene acetonitrile radical reaction is given in Fig. 2.

3.2 Chemical properties and structural elucidation of N-FG

The UV-Vis absorption spectrum of N-FG shows a plasmon peak near 214 nm, which is attributed to the conjugative and electron (π-π^*) shift of 1,3-diene present in the terminal graphene layer (-CH=CH-CH=CH-).[30] The strong electron donating and withdrawing (via resonance and inductive effects) properties of pyrrolic (-NH) and pyridinic (-N=CH-) nitrogen in N-FG shows absorption peaks at 215, 225, 239, and 251 nm.[36, 37] The absorption bands at 261 and 272 nm are attributed to electronic conjugation within the N-FG layer.[7, 38] UV-Vis absorption spectra for acetonitrile and N-FG are given in Fig. 3b. The fluorescence spectrum of N-FG exhibits a strong fluorescence intensity at 558 nm due to the increase in π-π^* electronic transition, and confirms the presence of fluorophores such as -NH and -N=CH- within the reduced graphene sheet.[30, 39] The fluorescence spectrum of N-FG is given in the inset of Fig. 3b. The FT-IR spectrum of the N-FG composite is given in Fig. 3a. The CH in-plane bending vibrations usually occur in the region of 1430-990 cm^{-1}.[40, 41] N-FG shows bands at 986 and 1068 cm^{-1}, which are attributed to δ(C-H) bending vibration. The methyl-substituted carbon-carbon γ(C=C) stretching vibration appears at 1425, 1462, 1631, and 1656 cm^{-1} (=CH).[42, 43] Peaks around 2854 and 2927 cm^{-1} correspond to asymmetric and symmetric -CH stretching modes, respectively. Bands corresponding

to 1425 and 1462 cm^{-1} are attributed to C-H bending vibration (aromatic C-H bending vibration).[44] Bands corresponding to 2045, 2208, and 3468 cm^{-1} are attributed to -CH=N and -CH-NH groups, which are possible in a ring-like structure.[30, 44] The coexistence of pyridinic and pyrrolic nitrogen within N-FG shows the significant dispersibility of N-FG in polar and non-polar solvents.

Raman spectroscopy was carried out to evaluate the degrees of structural distortion of N-FG and graphite (Fig. 3c). The Raman spectra of graphite and N-FG show the disordered sp^3 D band at 1332 and 1330 cm^{-1}, respectively.[45] Similarly, the E_{2g} vibrational mode in the sp^2 carbon (G band) appears at 1573 and 1580 cm^{-1} for graphite and N-FG, respectively.[46] The increase in the D band intensity of N-FG (breathing modes of A_{1g} symmetry) is indicative of the degree of short-range disorder, such as in-plane substitutional heteroatoms, vacancies, and grain boundaries. The inset of Fig. 3c shows the ID/IG ratios of graphite and N-FG, which are 0.593 and 0.81, respectively. The higher ID/IG ratio of N-FG is a result of structural defects caused by the nitrogen heteroatoms or groups implanted at the radicalized graphene site. The insertion of nitrogen groups increases the sp^3 carbon in graphene and changes the hybridization and symmetry of N-FG.[47, 48] The 2D band appears at 2683 and 2656 cm^{-1} for graphite and N-FG, respectively. The 2D band is related to disorder-induced defects, but it is seen even in non-disordered systems and its shape is highly sensitive to the number of graphene layers.[49, 50] The 2D/G ratio is 1.2 for N-FG, indicating the formation of a few layers of functionalized graphene in the SLP process.[51] Hence, the defects in the N-FG layers increase the D peak intensity and exhibit the reduction trend to the 2D and G peak intensities. Hence, the distortion caused by the insertion of nitrogen groups is confirmed by Raman analysis. HR-TEM images show the presence of single to few-layer N-FG (Fig. S2) ($n < 5$) and small

flakes stacked at the bottom (Figs. 4a and 4b). The defects caused by micro-plasma discharge can be clearly observed in N-FG sp^2 domains (Fig. 4c). The formation of single-layer N-FG in the SLP process is further confirmed by selected-area electron diffraction (SAED) (Fig. 4d).

XPS measurements were carried out to determine the level of nitrogen introduced into N-FG. The XPS spectra of graphite before and after the SLP process are given in Fig. S2. The XPS spectrum of pure graphite shows peaks at binding energies of 284.5 and 533.1 eV, which are ascribed to C1s and O1s. Similarly, the spectrum of N-FG shows peaks at binding energies of 284.4, 398.5, and 532.8 eV (Fig. S3). The O1s peak is considered to be from adsorbed molecular oxygen on pure graphite.[52] The XPS spectrum shows 4.2% nitrogen in N-FG. The electronic 1s core levels of N and C for graphite and N-FG were analyzed and numerically fitted with Gaussian functions. The C 1s region of pure graphite consists of a well resolved binding energy configuration at 284.7 eV, attributed to sp^2 carbon (Fig. 4e).[46, 50, 53] Similarly, the C 1s region of N-FG (Fig. 4f) has two well resolved binding energy configurations, namely at 284.3 and 285.0 eV, attributed to sp^2 carbon, and a new peak at 285.0 eV due to the presence of distorted sp^3 carbon ($-CH_2$ and C-N) present in N-FG.[54, 55] The N 1s region of N-FG (Fig. 4g) has two broad peaks at 398.1 and 399.3 eV, which can be attributed to the C-N or -C-NH and -C=N- bonds, respectively.[30, 54-56] The nitrogen present in the form of -C=N- can exist only in the pyridine ring-like structure.[51, 53] The binding energies of the above assigned groups are in good agreement with the UV-Vis, fluorescence spectroscopy, and FT-IR analyses.

3.3 Electrochemical properties of N-FG

The electrochemical properties of N-FG were evaluated in a three-electrode system.

The two sequential oxidation and reduction waves observed in CV (Fig. 5a) at scan rates of 5, 25, 50, and 100 mV/s correspond to pyridinic and pyrrolic nitrogen, respectively. The second oxidation and reduction peaks are small, and at high scan rates (50 and 100 mV/s), the reduction peaks completely merge, producing a single peak. The distinct redox peaks were observed even at high scan rates and are attributed to the pyrrolic (-C-NH), and pyridinic (-C=N-) nitrogen present in N-FG.[10] Possible oxidation and reduction reactions are:

$$(\text{Pyrrolic N}) — \text{CH} — \text{NH} \leftrightarrow N - FG — \text{C} = \text{N}^+ + e^- \quad (1)$$

$$(\text{Pyridinic N}) — \text{C} = \text{N} — \leftrightarrow N - FG — \text{C} = \text{N}^+ — + e^- \quad (2)$$

The difference between the potentials of anodic (E_{pa}) and cathodic (E_{pc}) peak currents was found to be (ΔE_p) 78, 97, 105, and 123 mV at scan rates of 5, 25, 50, and 100 mV/s, respectively. The increase in ΔE_p is due to the resistive effect of the N-FG electrode and clearly indicates a marginal reduction in the electron transfer rates at high scan rates. The pyridinic nitrogen present in N-FG undergoes a controlled oxidation reduction reaction even at the high scan rates, whereas the highly electronegative pyrrolic nitrogen reduces the electron transfer rate at high scan rates.[18, 21] The marginal reduction in the electron transfer rate of N-FG clearly indicates that the redox reaction is predominately controlled by pyridinic nitrogen.[57] Furthermore, electrochemical performance of N-FG is also influenced by the nitrogen content, disorders or defects caused by sp^3 carbon, and electrode/electrolyte wettability.[21] The anodic and cathodic peak currents of N-FG at various scan rates show a linear relationship with the square root of the scan rate (Fig. 5c) and are in good agreement with the Randles-Sevcik equation.[58] The specific capacitance values of N-FG are 291, 177, 151, and 131 F/g for scan rates of 5, 25, 50, and 100 mV/s, respectively. The decrease in specific capacitance values is due to the decrease in the electron transfer

rate. Similar distinct redox peaks (faradic) have been observed for the graphene oxide-polyaniline and graphene oxide-conjugated polymer (poly-3,4-propylenedioxythiophene) composites, whose specific capacitances are 525 and 201 F/g, respectively.[12, 14] The N-FG electrode shows high cyclic stability and a high degree of reversibility at a scan rare of 100 mV/s. The capacitive current response remains unchanged at the end of 1000 cycles, and only a <10 % reduction of the specific capacitance was observed (Fig. 5b).

4. Conclusion

The formation of N-FG via a solution process is a potential alternative to high-temperature synthesis. Advantages of the SLP process include simple setup, minimal surface damage due to fast moving electrons, no required further purification, possible large-scale synthesis, low operating cost, and eco-friendliness. The ·H and $\cdot CH_2\text{-}C \equiv N$ radicals are highly selective and form covalent bonds at the radicalized sites of carbon, restoring partial aromaticity by extending conjugation with neighboring atoms. The insertion of pyridinic (-C=N-) and pyrrolic (-C-NH) nitrogen enhances the dispersibility and electrocapacitive properties of N-FG. The nitrogen groups present in N-FG lead to a high specific capacitance (291 F/g) and high cyclic stability. N-FG could be further modified for high-performance supercapacitor, energy storage, sensor, and solar cell applications.

Acknowledgements

The authors are grateful to Prof. Yury Gogotsi, Department of Materials Science and Engineering and A. J. Drexel Nanotechnology Institute, Drexel University for providing discussion and support. The authors gratefully acknowledge the support of

Prof. Jiunn-Der Liao (Department of Material Science and Engineering, National Cheng Kung University), Prof. Wen-Ta Tsai, and Prof. Jih-Jen Wu for help and discussion regarding experiments.

References

1. K. S. Novoselov, V. I. Fal'ko, L. Colombo, P. R. Gellert, M. G. Schwab and K. Kim, *Nat.*, 2012, **490,** 192-200.
2. R. Ruoff, *Nat. Nanotech.*, 2008, **3,** 10-11.
3. F. Bonaccorso, A. Lombardo, T. Hasan, Z. Sun, L. Colombo and A. C. Ferrari, *Mater Today.*, 2012, **15(12),** 564-589.
4. P. Simon and Y. Gogotsi, *Nat. Mater.*, 2008, **7,** 845-854.
5. D. Li, M. B. Müller, S. Gilje, R. B. Kaner and G. G. Wallace, *Nat. Nanotech.*, 2008, **3,** 101-105.
6. S. Stankovich, D. A. Dikin, G. H. B. Dommett, K. M. Kohlhaas, E. J. Zimney, E. A. Stach, R. D. Piner, S. T. Nguyen and R. S. Ruoff, *Nat.*, 2006, **442,** 282-286.
7. S. J. Woltornist, A. J. Oyer, J-M. Y. Carrillo, A. V. Dobrynin and D. H. Adamson, *ACS Nano,* 2013, **7(8),** 7062-7066.
8. V. Georgakilas, M. Otyepka, A. B. Bourlinos, V. Chandra, N. Kim, K. C. Kemp, P. Hobza, R. Zboril and K. S. Kim, *Chem. Rev.*, 2012, **112,** 6156-6214.
9. Q. Wu, Y. Xu, Z. Yao, A. Liu and G. Shi, *ACS Nano,* 2010, **4,** 1963-1970.
10. H. Filik, G. Çetintaş, A. A. Avan, S. N. Koç and I. Boz, *Int. J. Electrochem. Sci.*, 2013, **8,** 5724-5737.
11. Y. Xu, Z. Liu, X. Zhang, Y. Wang, J. Tian, Y. Huang, Y. Ma, X. Zhang and Y. *Chen, Adv. Mater.*, 2009, **21,** 1275-1279.
12. N. A. Kumar, H. J. Choi, A. Bund, J. B. Baek and Y. T. Jeong, *J. Mater. Chem.*, 2012, **22,** 12268-12274.
13. Y. Lu, F. Zhang, T. Zhang, K. Leng, L. Zhang, X. Yang, Y. Ma, Y. Huang, M. Zhang and Y. Chen, *Carbon*, 2013, **63,** 508-516.
14. Y. Liu, R. Deng, Z. Wang and H. Liu, *J. Mater. Chem.*, 2012, **22,** 13619-13624.
15. B. You, L. Wang, L. Yao and J. Yang, *Chem. Commun.*, 2013, **49,** 5016-5018.
16. H. Liu, Y. Liu and D. Zhu, *J. Mater. Chem.*, 2011, **21,** 3335-3345.
17. Y. Liang, F. Liang, H. Zhong, Z. Li, R. Fu and D. Wu, *J. Mater. Chem. A*, 2013, **1,** 7000-7005.

18. H. Wang, T. Maiyalagan and X. Wang, *ACS Catal.*, 2012, **2,** 781-794.

19. Y. Fang, B. Luo, Y. Jia, X. Li, B. Wang, Q. Song, F. Kang and L. Zhi, *Adv. Mater.*, 2012, **24,** 6348-6355.

20. L. Qu, Y. Liu, J-B. Baek and L. Dai, *ACS Nano,* 2010, **4(3),** 1321–1326.

21. C. Wang, Y. Zhou, L. He, T. W. Ng, G. Hong, Q. H. Wu, F. Gao, C. S. Lee and W. Zhang, *Nanoscale*, 2013, **5,** 600-605.

22. C. Zhang, L. Fu, N. Liu, M. Liu, Y. Wang and Z. Liu, *Adv. Mater.*, 2011, **23,** 1020-1024.

23. Z. H. Sheng, L. Shao, J. J. Chen, W. J. Bao, F. B. Wang and X. H. Xia, *ACS Nano*, 2011, **5(6),** 4350-4358.

24. Z. Dai, K. Wang, L. Li and T. Zhang, *Int. J. Electrochem. Sci.*, 2013, **8,** 9384-9389.

25. D. Deng, X. Pan, L. Yu, Y. Cui, Y. Jiang, J. Qi, W. X. Li, Q. Fu, X. Ma, Q. Xue, G. Sun and X. Bao, *Chem. Mater.*, 2011, **23(5),** 1188-1193.

26. L. Guan, L. Cui, K. Lin, Y. Y. Wang, X. T. Wang, F. M. Jin, F. He, X. P. Chen and S. Cui, *Appl. Phys. A*, 2011, **102,** 289-294.

27. H. L. Poh, P. Simek, Z. Sofer, I. Tomandlc, M. Pumera, *J. Mater. Chem. A*, 2013, **1,** 13146-13153.

28. F. Bonaccorso, A. Lombardo, T. Hasan, Z. Sun, L. Colombo and A. C. Ferrari, *Mater. Today,* 2012, **15(12),** 564-589.

29. S. Park and R. S. Ruoff, *Nat. Nanotech.*, 2009, **29(4),** 217-224.

30. J. Senthilnathan, C. C. Weng, J. D. Liao and M. Yoshimura, *Sci. Rep.*, 2013, **3,** 2414-2420.

31. H. Wang and M. Yoshimura, *Chem. Phys. Lett.*, 2001, **348,** 7-10.

32. T. Watanabe, H. Wang, Y. Yamakawa and M. Yoshimura, *Carbon*, 2006, **44,** 799-823.

33. C. C. Weng, J. C. Hsueh, J. D. Liao, C. H. Chen and M. Yoshimura, *Plasma Processes Polym.*, 2013, **10,** 345-352.

34. N. Inagaki, S. Tasaka and Y. Yamada, *J. Polym. Sci. Part A Polym. Chem.*, 1992, **30(9),** 2003-2010.

35. N. Inagaki, Plasma surface modification and plasma polymerization, Technomic

Publishing Company, Lancaster, PA, 1996.

36. M. Jahan, Q. Bao and K. P. Loh, *J. Am. Chem. Soc.*, 2012, **134,** 6707-6713.

37. N. U. Sri, K. Chaitanya, M. V. S. Prasad, V. Veeraiah and A. Veeraiah, *Spectrochim. Acta Mol. Biomol. Spectros.*, 2012, **97,** 728-736.

38. G. A. Rance, D. H. Marsh, R. J. Nicholas and A. N. Khlobystov, *Chem. Phys. Lett.*, 2010, **493,** 19-23.

39. J. Shi, W. Xu, Q. Liu, F. Liu, Z. Huang, H. Lei, W. Yu and Q. Fang, *Chem. Commun.* 2002, **7(7),** 756-757.

40. M. Karabacak, Z. Cinar, M. Kurt, S. Sudha and N. Sundaraganesan, *Spectrochimica Acta Part A*, 2012, **85(1),** 179-189.

41. P. B. Nagabalasubramanian, M. Karabacak and S. Periandy, *Spectrochimica Acta Part A*, 2011, **82(1),** 169-180.

42. T. D. Savi´c, Z. V. Saponji´c, M. I. Comor, J. M. Nedeljkovi´c, M. D. Drami´canin, M. G. Nikoli´c, D. Ž. Veljković, S. D. Zarić and I. A. Janković, *Nanoscale*, 2013, **5,** 7601-7612.

43. M. Silverstein, G. C. Basseler and C. Morill, Spectrometric identification of organic compounds. Wiley, New York, USA, 1981.

44. Y. Q. Zhan, R. Zhao, F. B. Meng, Y. J. Lei, J. C. Zhong, X. L. Yang and X. Liu, *Sci. Eng. B*, 2011, **176,** 779-784.

45. S. W. Lee, C. Mattevi, M. Chhowalla and R. M. Sankaran, *J. Phys. Chem. Lett.*, 2012, **3,** 772-777.

46. N. A. Kumar, H. Nolan, N. McEvoy, E. Rezvani, R. L. Doyle, M. E. G. Lyons and G. S. Duesberg, *J. Mater. Chem. A*, 2013, 1, 4431-4435.

47. D. C. Elias, R. R. Nair, T. M. G. Mohiuddin, S. V. Morozov, P. Blake, M. P. Halsall, A. C. Ferrari, D. W. Boukhvalov, M. I. Katsnelson, A. K. Geim and K. S. Novoselov, *Science*, 2009, **323,** 610-613.

48. M. Chen, H. Zhou, C. Qiu, H. Yang, F. Yu and L. Sun, *Nanotech.*, 2012, **23,** 115706.

49. J. G. Zhou, J. Wang, C. L. Sun, J. M. Maley, R. Sammynaiken, T. K. Sham and W. F. J. Pong, *Mater. Chem.*, 2011, **21,** 14622-14630.

50. A. L. M. Reddy, A. Srivastava, S. R. Gowda, H. Gullapalli, M. Dubey and P. M.

Ajayan, *ACS Nano*, 2010, **4,** 6337-6342.

51. A. C. Ferrari, *Solid State Commun.*, 2007, **143,** 47-57.
52. C. He, S. P. Jiang and P. K. Shen, *Sci. Rep.*, 2013, **3,** 2144-2149.
53. Y. Wang, Y. Shao, D. W. Matson, J. Li and Y. Lin, *ACS Nano*, 2010, **4,** 1790-1798.
54. A. P. Dementjev, A. de-Graaf, M. C. M. van-de Sanden, K. I. Maslakov, A. V. Naumkin and A. A. Serov, *Diam. Relat. Mater.* 2000, **9,** 1904-1907.
55. G. P. Mane, S. N. Talapaneni, C. Anand, S. Varghese, H. Iwai, Q. Ji, K. Ariga, T. Mori and A. Vinu, *Adv. Funct. Mater.*, 2012, **22,** 3596-3604.
56. A. Johanson and S. Stafstrom, *J. Chem. Phys.*, 1999, **111,** 3203-3208.
57. K. Gong, F. Du, Z. Xia, M. Durstock and L. Dai, *Science*, 2009, **323,** 760-763.
58. N. G. Shang, P. Papakonstantinou, M. McMullan, M. Chu, A. Stamboulis, A. Potenza, S. S. Dhesi and H. Marchetto, *Adv. Funct. Mater.*, 2008, **18,** 3506-3514.

Figure Captions

Fig. 1 Comparison of high-temperature synthesis methods of nitrogen-doped graphene

Fig. 2 Proposed mechanism for the formation of nitrogen-functionalized graphene in SLP. (i) micro plasma discharge facilitates the exfoliation of radicalized graphene layer in the acetonitrile solution (ii) electron generated in micro plasma discharge collision with acetonitrile and forms nascent hydrogen and acetonitrile radicals (iii) formation of N-FG by the reaction of radicalized graphene layer with nascent hydrogen and acetonitrile radicals

Fig. 3 (a) FT-IR spectra of N-FG, (b) UV-Vis spectra of (i) acetonitrile and (ii) N-FG, and (c) Raman spectra of (i) graphite and (ii) N-FG

Fig. 4 (a-c) HR-TEM images of N-FG and XPS spectra of (d) SAED pattern of N-FG (e) graphite C 1s region, (f) N-FG C 1s region, and (g) N-FG N 1s region

Fig. 5 (a) Electrochemical CV curves of N-FG in 6 M KOH obtained at scan rates of 5, 25, 50, and 100 mV/s. (b) Cycle stability of composite at scan rate of 100 mV/s. (c) Peak current dependence on the square root of scan rate. Note: C. density = Current density

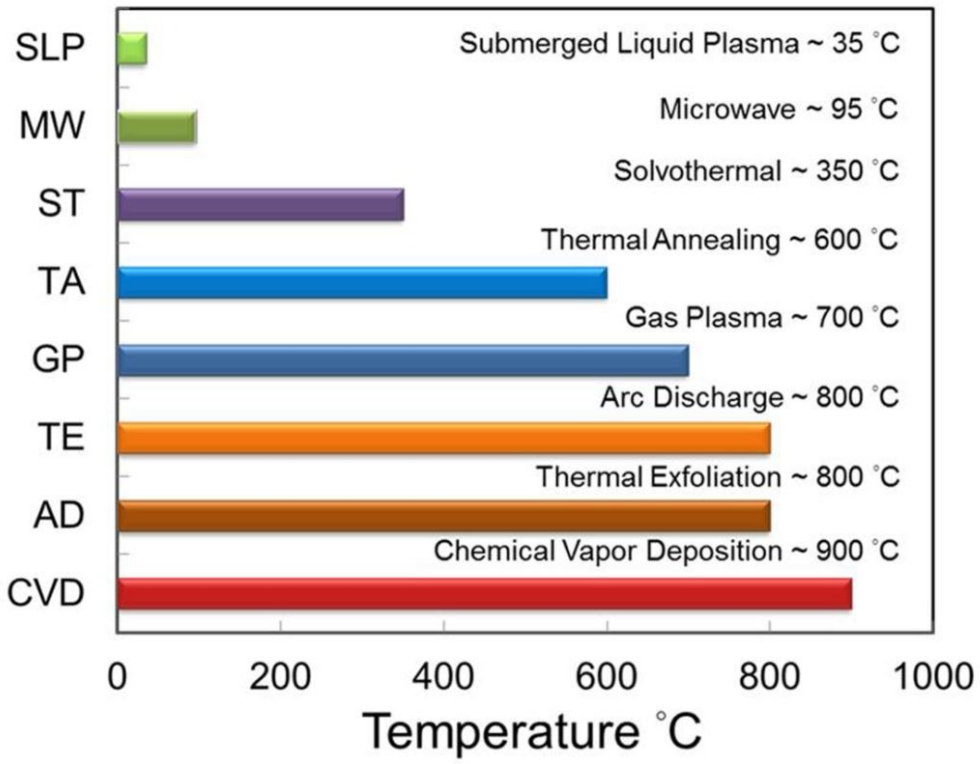

Fig. 1

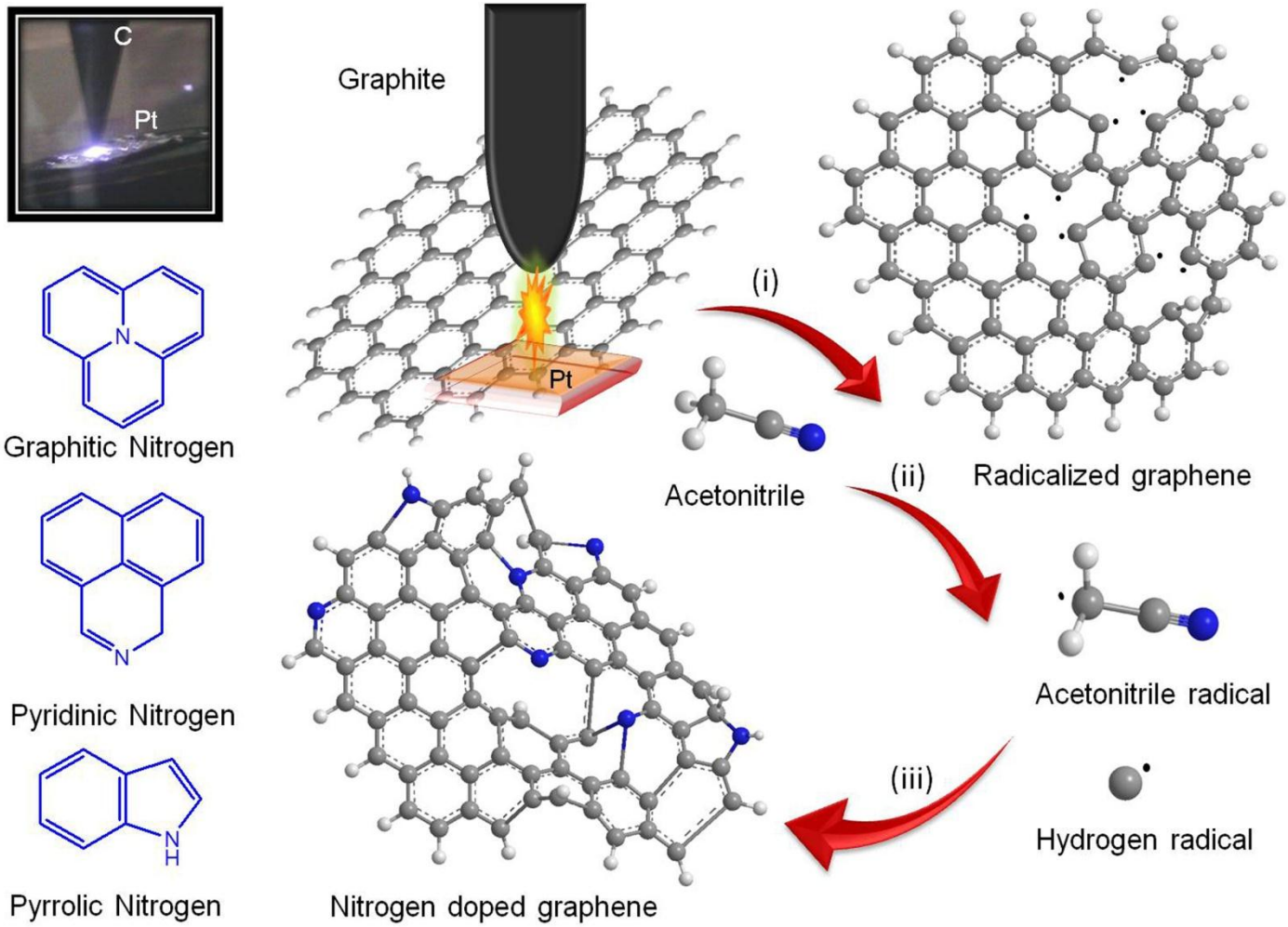

Fig. 2

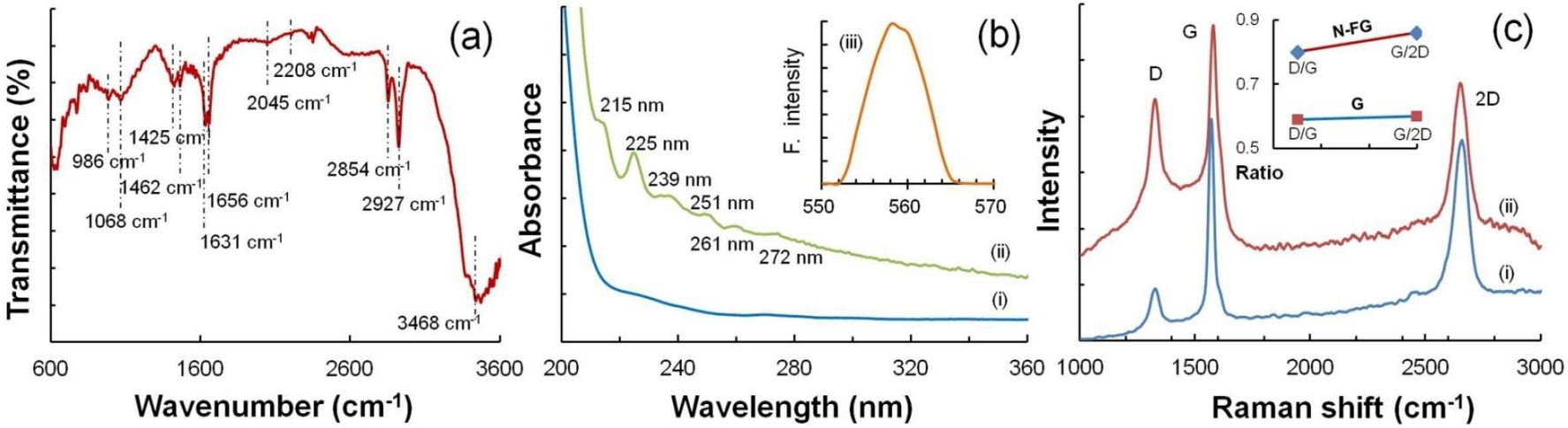

Fig. 3

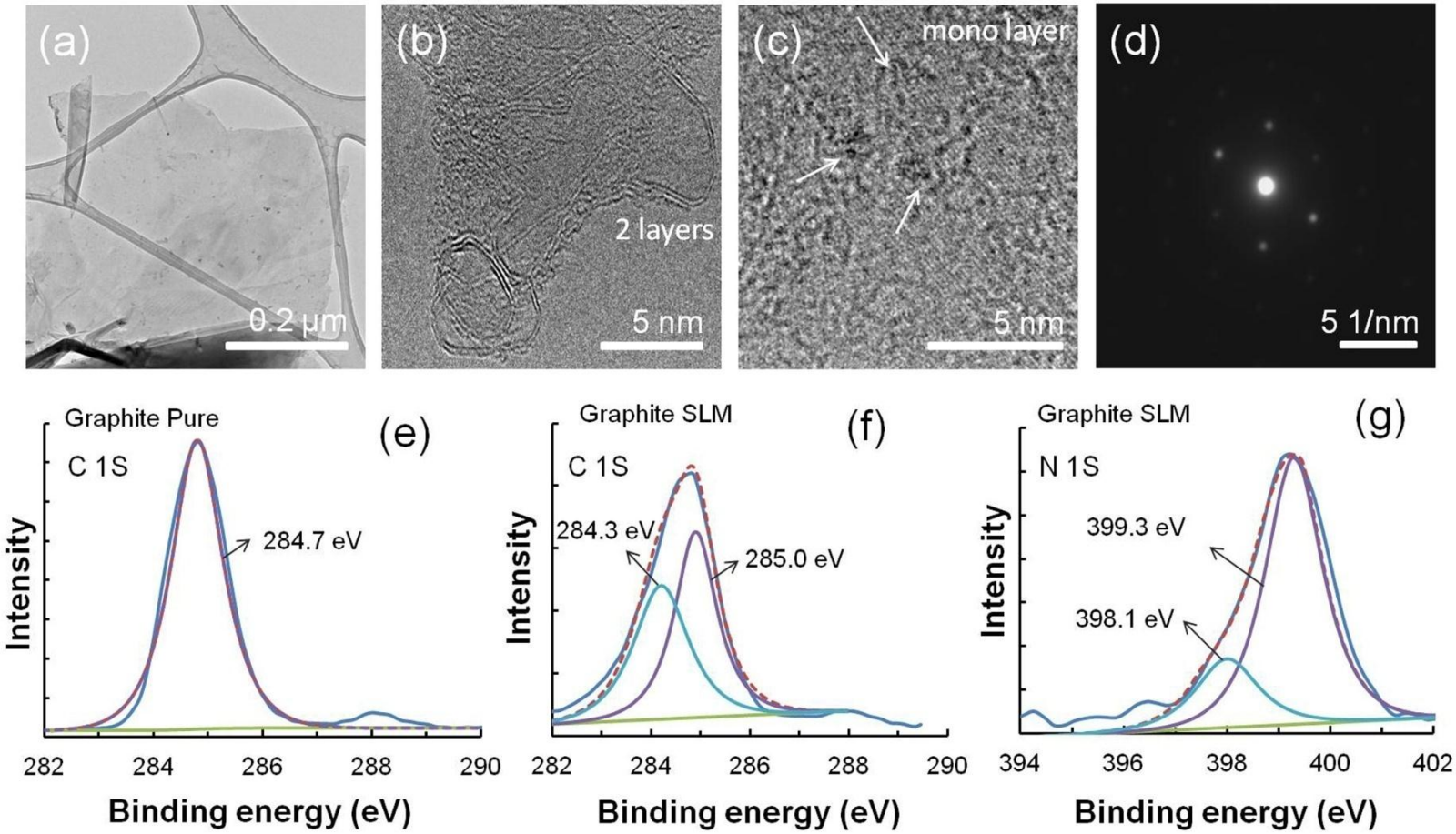

Fig. 4

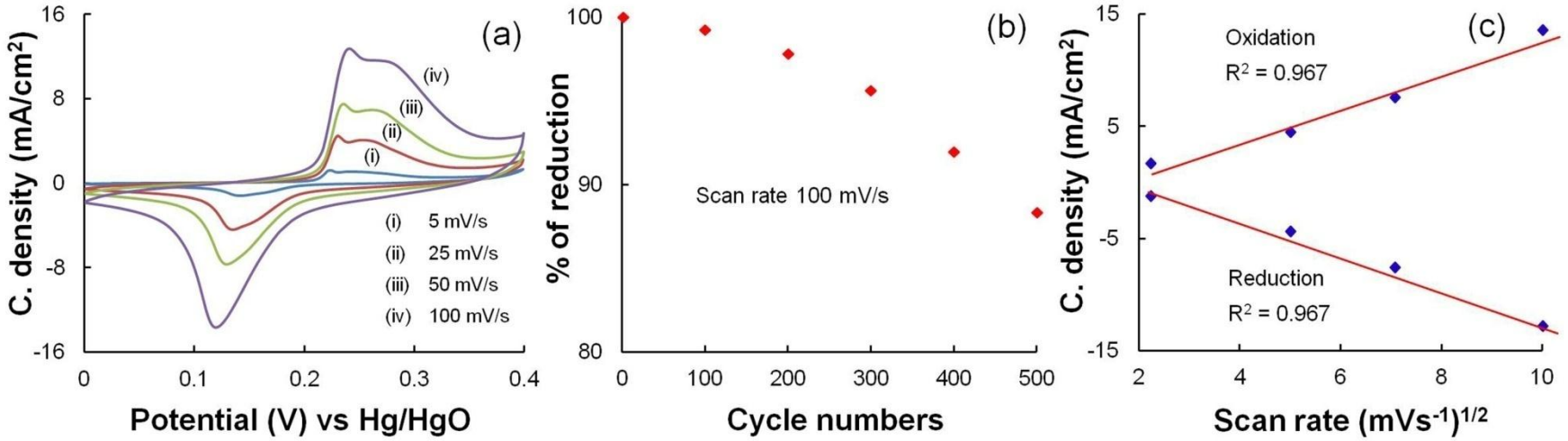

Fig. 5